University of Michigan's Upgraded Large Vacuum Test Facility

IEPC-2019-653

Presented at the 36th International Electric Propulsion Conference
University of Vienna • Vienna, Austria
September 15-20, 2019

Eric A. Viges[1], Benjamin A. Jorns[2], Alec D. Gallimore[3] and J. P. Sheehan[4]
University of Michigan, Ann Arbor, 48105, USA

Abstract: Recent upgrades to the pumping speed of the Large Vacuum Test Facility (LVTF) at University of Michigan are presented. These upgrades are in response to two growing needs in electric propulsion testing capabilities: the need for higher pumping speed to test higher power electric propulsion and the need to achieve lower operating pressures for studying the role of pressure-related facility effects influencing the operation of state of the art systems. Previously, the LVTF had seven PHPK-TM1200i re-entrant cryogenic vacuum pumps that provided an effective pumping speed of ~190,000 l/s for xenon. The upgraded facility has thirteen PHPK-TM1200i and six PEPL-developed-cryopumps which make use of the Cryomech AL600 Gifford-McMahon cryocooler. The PEPL cryopump is a liquid nitrogen free cryopump that has a theoretical pumping speed of 39,600 l/s for xenon. The upgraded facility has a measured effective pumping speed of 500,000 l/s for xenon for operating high power thrusters and 600,000 l/s for xenon cold flow measurements. For krypton, the facility has an effective pumping speed of 600,000 l/s for an operating thruster and 660,000 l/s for cold flow measurements.

Nomenclature

S_{th}	=	theoretical cryopumping speed
A	=	area of pumping plate
T_i	=	incident gas temperature to the condensing surface (pumping plate)
M	=	molecular weight of condensing gas
R	=	ideal gas constant
T_c	=	temperature of the pumping plate
P_c	=	vapor pressure of the condensing gas
Pi	=	pressure of the incident gas
n_{ig}	=	ion gauge neutral density
n_{ch}	=	chamber neutral density
T_{ig}	=	gas temperature inside ion gauge
T_{ch}	=	gas temperature inside chamber

[1] Senior Research Engineer, University of Michigan, eviges@umich.edu
[2] Assistant Professor, Department of Aerospace Engineering
[3] Robert J. Vlasic Dean of Engineering
[4] Assistant Research Scientist, Aerospace Engineering (previously)

I. Introduction

THE Large Vacuum Test Facility (LVTF) in the Plasmadynamics and Electric Propulsion Laboratory (PEPL) at the University of Michigan (UM) has been upgraded to support next generation electric propulsion (EP) devices. Notable past examples of EP devices tested at the LVTF include the NSTAR gridded ion thruster[1], Fakel's SPT-100[2] as well as Aerojet Rocketdyne's XR-5 and XR-12 Hall Effect Thrusters (HET).[3] More recently, the LVTF has served as the testbed for the development of the X3, a record-breaking 100 kW-class nested HET[4] and the H9, a 9 kW magnetically shielded HET[5].

The previous effective pumping speed of the LVTF was ~190,000 l/s (190 kl/s) on xenon. This was provided by seven PHPK TM1200i re-entrant cryopumps. For the past two decades, this pumping speed was thought to be sufficient to test state of the art electric propulsion systems (i.e. those operating below 5 kW), while maintaining facility backpressure below the industry-recommended upper bound of 13 µTorr for near field plume measurements.[6] There have been two recent developments in the electric propulsion field that created a need for increasing the LVTF's pumping capability. First, advances in space solar panel and thruster technology are enabling higher power electric propulsion systems that output 2-3 times more propellant than their lower- power predecessors[7,8,9]. There has been increased interest from government and industry to support developments and test campaigns involving higher power devices (i.e. those operating above 5 kW). In order to operate these next generation systems below the industry-recommended guidelines in the LVTF, there was a need to have a commensurate 2-3 times factor increase in pumping speed (~ 500 kl/s). The upgraded facility is now better capable of testing these higher power systems. Second, experimental work has shown that there are new and unexplained effects of increasing facility backpressure on thruster performance.[10,11,12,13,14] This latter development in particular raises concerns about the validity of translating testing results from ground-based facilities to on-orbit behavior. Given this potential issue, there is renewed interest in understanding both analytically and experimentally the effects of changing facility pressure on thruster operation. This type of study requires a highly-variable facility, capable of high-pumping speed.

Although there are some existing chambers—most notably the L3 facility and the VF-5 Chamber at NASA Glenn Research Center—capable of providing the required pumping speeds (> 500, kl/s for xenon), there are currently no academic chambers that operate at this level. In light of the significant role academia will have in the study, design, and development of next-generation EP technology, this is a capability gap that should be closed. To this end, the goal of this effort has been to upgrade the LVTF at the University of Michigan to be capable of testing next-generation systems by increasing the pumping speed by a factor of nearly three. This effort has involved the installation of new cryogenic pumps, in-house development of a new cryogenic pump for pumping xenon and krypton, the modification of the facility to accommodate these new pumps, and the upgrade of the infrastructure to support the expanding cryopumping systems. Figure 1 shows a cutaway CAD model with new cryopumps colored red and previously existing pumps colored in blue as well as a photograph of the internal view of the upgraded chamber.

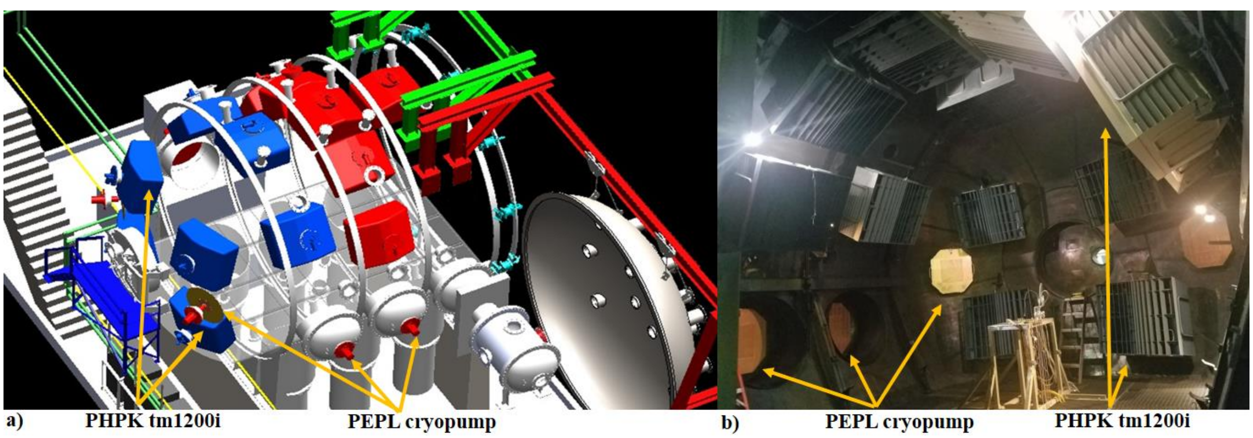

Figure 1. Cutaway CAD model (a) of the upgraded LVTF showing locations of each of the new cryopumps in red and the previously existing cryopumps in blue. Photo (b) LVTF from perspective of the beam dump.

This paper details the work performed to upgrade the chamber. In the first section, we overview LVTF and present the theory guiding pumping speed calculations and the development of the PEPL cryopump. In the second section, we cover the overview of the upgraded facility as well as the development of the PEPL cryopump. In the final section, we examine performance of the upgraded LVTF as well as the performance of the PEPL cryopump.

II. Background

A. Effective pumping speed calculation considerations

All pumping speed calculations were performed based on the procedures and guidelines in contained in reference 6. The mass flow calculations use a temperature of 298 K for both flow (sccm) and for pumping speed (l/s). A Granville-Phillips Stabil-ion gauge series 370 with controller were used for all reported pressure measurements. The gauges are calibrated on xenon. Measurements on krypton or xenon use proper ion gauge correction factors. The gauge assembly shown in Fig. 2 was mounted at the thruster exit plane for effectively pumping speed measurements. Flow meter calibrations were verified with a Bios dry calibration system.

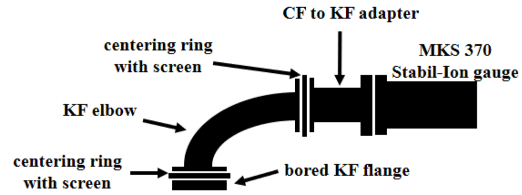

Figure 2. PEPL's gauge envelope design.

B. A physically compact and high-pumping-speed, LN_2 free cryopump for xenon and krypton

The PHPK TM1200i is one of the highest pumping speed standalone cryopumps available on the market today and has a theoretical pumping speed of 35 kl/s for xenon. Prior to the upgrade, the LVTF had used seven TM1200i cryopumps providing approximately 200 kl/s of effective pumping speed at the thruster. Due to the large size of this cryopump (115 cm × 135 cm × 94 cm), there were a limited number of additional locations that the cryopump could be physically fit within the LVTF. Considering the geometry constraints to the vacuum chamber, it was concluded that six additional TM1200i cryopumps could be added to the existing seven. These thirteen cryopumps thus delivering on the order of 300 to 400 kl/s of effective pumping speed. This fell short of the project target to exceed 500 kl/s and therefore additional options were explored. In order to reach the project target, it was concluded the PEPL would develop its own large cryopump based cryopump designs first demonstrated at JPL in the mid-1990s.[15] This cryopump would be designed to fit within smaller areas within the chamber such as the 48ASA flange caps. Since the LVTF had four empty 48ASA caps, if a large cryopump could fit within these caps, there would be potential to fit significantly more large pumps in the chamber.

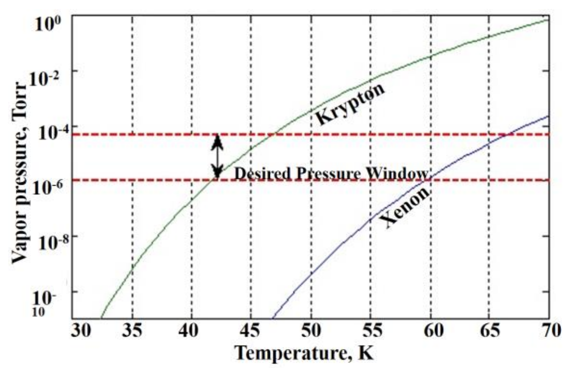

Figure 3. Vapor pressure curves for xenon and krypton.

The new cryopump, built by JPL is colloquially called "a thumper" due to the characteristic repetitive thumping noise produced by the cryocooler. JPL's cryopump design made use of newly developed high capacity single stage Gifford-McMahon (GM) cryocoolers available from Cryomech. In this design, the cryocooler would directly bolt to a pumping plate and conductive cool the plate down to temperatures sufficient to pump xenon, but not cold enough to pump nitrogen or oxygen. Due to the large capacity and higher temperature operation point, it was shown to be possible to design a cryopump without radiation baffling shielding the cold plate. This led to reductions in overall cost and complexity. In the baffle-less case, the condensed frozen xenon would be directly exposed to room temperature thermal radiation and still remain solidly condensed onto to the pumping plate. As shown in Fig. 3, in order to cryopump xenon gas down to a vapor pressure of 1 µTorr requires that the pumping surface be 60 K or colder. Similarly, krypton propellant requires the pumping surface to be 43 K or less. As discussed in depth Garner et al. [15], the goal of any similar cryopump design is to match the cryocooler capacity curve and the conductivity of the pumping plate with the radiative thermal environment. An optimized design would achieve the largest plate possible that would remain cold enough at the plate edge to condense propellant. If the thermal gradient across the pumping plate became too large, the edge would no longer cryopump. If thermal gradients in the plate increased partway through a test, where gases that had already condensed at the edge and now were no longer stable, such propellant might be shed from the pumping plate as the edge rose above the required temperature. This shedding could cause pressure spiking events in the chamber as flakes of frozen xenon from the pumping plate flashed to gas. It is important to note that radiation is the dominant heat transfer that is occurring in the system and the heat of fusion of the condensing propellant produces relatively insignificant thermal load. It also needs to be considered that while a clean pumping plate has low emissivity and therefore does not absorb significant radiation, as soon as propellant ice is condensed upon the plate, the emissivity rapidly increases. It is therefore reasonable to assume emissivity of one for a conservative and robust thermal design of the pumping plate.

JPL's initial cryopumps were based upon the AL200 Cryomech which has around 100 W cooling at 50 K[16]. Since that work was completed, larger GM cryocoolers are available. For this effort, the goal was set to design a compact liquid nitrogen (LN_2) free cryopump that could pump both xenon and krypton that matched or exceeded the pumping performance of a TM1200i. The PEPL cryopump would be based around the AL600 Cryomech, the largest single stage GM cryocooler available from Cryomech. As shown in Fig 4., the AL600 cryocooler has a capacity of 350 Watts at 50K or 250 Watts at 40K, the temperatures required for pumping xenon and krypton gases respectively down to a partial pressure of 1 µTorr. As shown in Eq. 1 maximum theoretical pumping speed of a cryopump (S_{th}) is dependent on the area (A) of the cold surface, the incident gas temperature (T_i), which in this case is assumed to be 298 K, the ideal gas constant (R), temperature of the condensing surface (T_c), the pressure of the incident gas (P_i), the vapor pressure of the condensed gas (P_c), and the molecular weight of that gas (M) as,

$$S_{th} = A\sqrt{\frac{T_i R}{2\pi M}}\left[1 - \frac{P_c}{P_i}\sqrt{\frac{T_i}{T_c}}\right] \qquad (1)$$

Assuming that ratio of P_c/P_i is small due to a sufficiently cold pumping plate (less than 55 K for Xe), the second half of Eq. 1 can be ignored. In this case, a square meter of exposed pumping plate will cryopump at a speed of 55 kl/s for xenon gas at room temperature. The goal for the PEPL cryopump design was to build a cryopump with greater pumping speed than a Tm1200i (35 kl/s). Based on the area specific pumping speed (55 kl/sm^2), in order to achieve better than 35 kl/s requires a cold plate with at least 0.63 square meters of pumping plate.

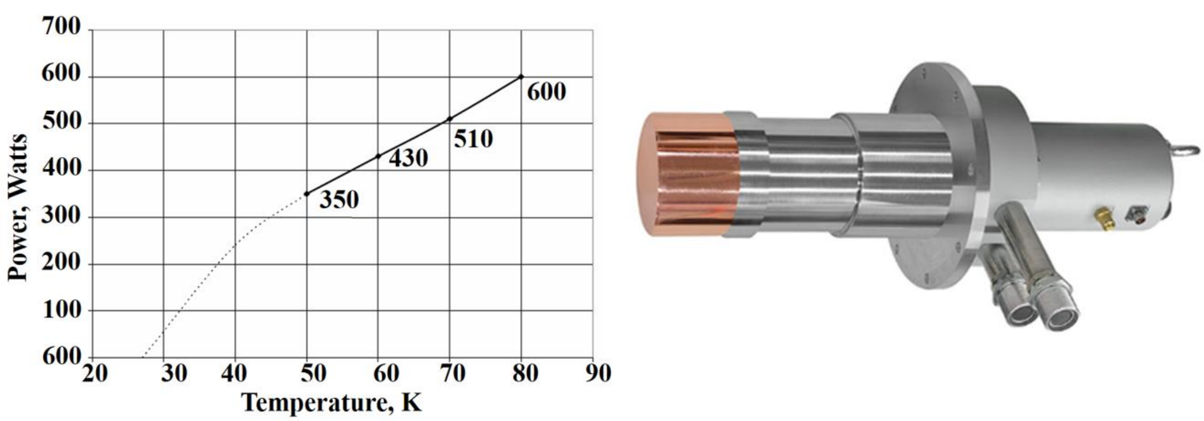

Figure 4. Cryomech's AL600 Gifford-McMahon cryocooler, cooling capacity curve adapted from manual.

C. Considerations for pumping various propellants at the LVTF

The PEPL cryopumps are not designed to reach temperatures low enough to cryopump nitrogen, oxygen, neon, hydrogen, or helium and therefore only the thirteen TM1200i cryopumps will be relevant for such propellants. They are designed to primarily pump both xenon and krypton, which as of writing this paper are the two most common electric propulsion propellants in use today. From Eq. 1, since pumping speed is inversely proportional to the square root of the molecular gas that is being pumped, the relative pumping speed of any condensable gas can be converted from the pumping speed of any another condensable gas. This is assuming of course that the cryopump is cold enough to effectively pump that gas. For purposes of these

Xenon has a molecular mass of 131.1 amu while krypton has a molecular mass 83.8 amu. Therefore, the relative pumping speed (volumetric) is approximately 1.25:1 krypton to xenon. Krypton gas should cryopump 25% faster than xenon on the same cryopump.

III. LVTF Upgrade Overview

A. The new LVTF vacuum pump configuration

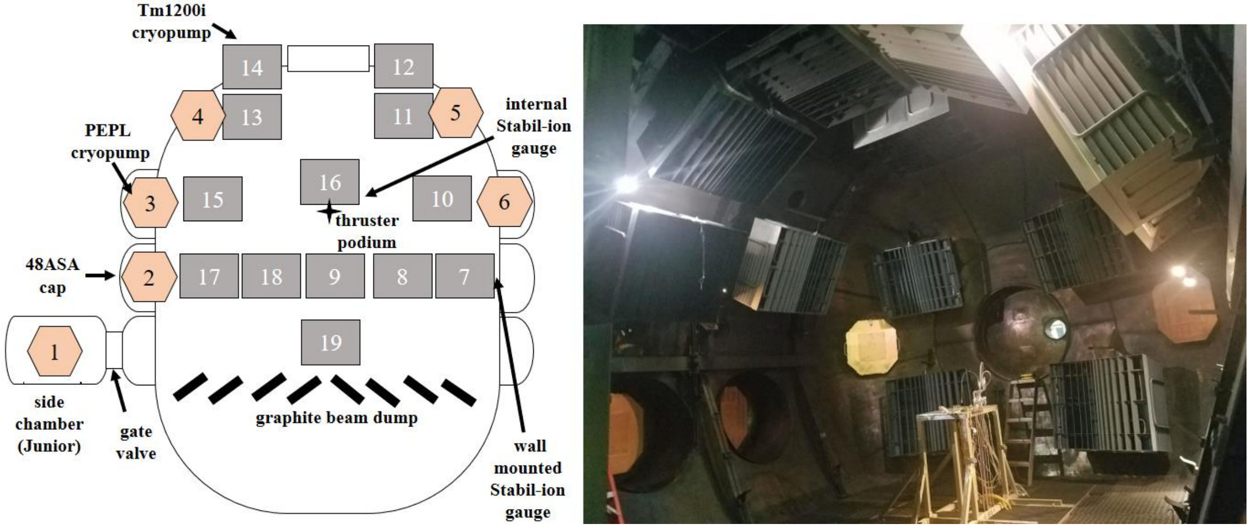

Figure 5. The upgraded LVTF configuration schematic (a) and the view from the beam dump (b).

Figure 5 shows the configuration of the upgraded LVTF and a photo of the competed chamber. Note that all of the cryopumps are visible in the photo except pumps numbers 6 and 19. The main vacuum chamber now has thirteen TM1200i and five PEPL cryopumps for a total of eighteen large cryopumps. Manufacturer specified pumping speed for the TM1200i cryopump is 35 kl/s, and the PEPL cryopumps have an exposed surface area of 0.72 m^2, leading to a theoretical pumping speed of 39.6 kl/s for xenon. Combining all of the contributions, the total installed pumping speed for this configuration is 653 kl/s for xenon. This total installed pumping speed is not the effective pumping speed at the thruster; however, it is useful for evaluating the efficiency of the pumping configuration and therefore is included. The internal Stabil-ion gauge is mounted off the thruster podium (also shown in Fig. 5) in line with the exit plane of the thruster. This is consistent with the EP best-practices paper (Dankanich). The beam dump is angled in the direction as is shown in the schematic. There is a second wall mounted Stabil-ion gauge mounted beneath cryopump number 7.

B. Infrastructure upgrades to support the new facility

The supporting infrastructure for the LVTF is shown in Fig 6. Electrical, LN_2 distribution, nitrogen exhaust, process water and pump telemetry systems are updated to support new cryopumps.

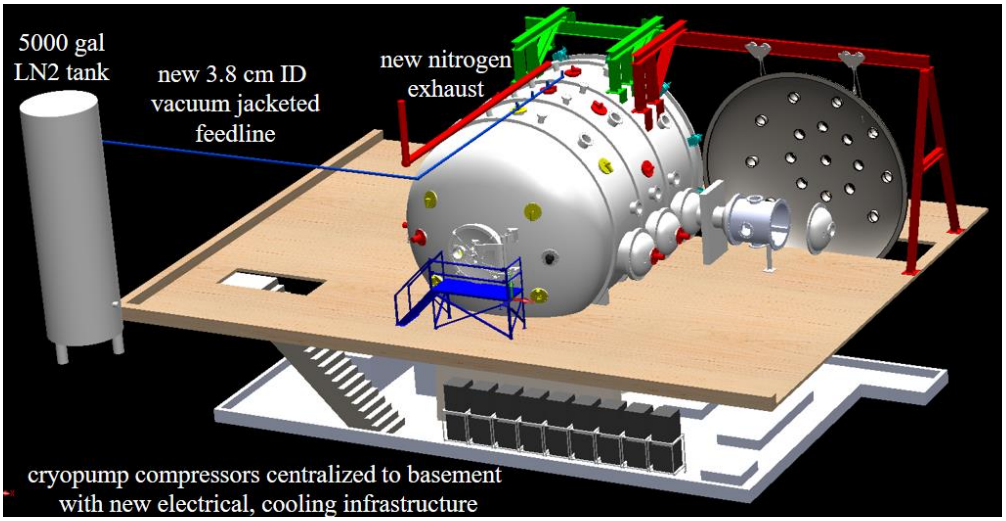

Figure 6. Upgraded support infrastructure including new vacuum jacket LN_2 feed line and N_2 exhaust line.

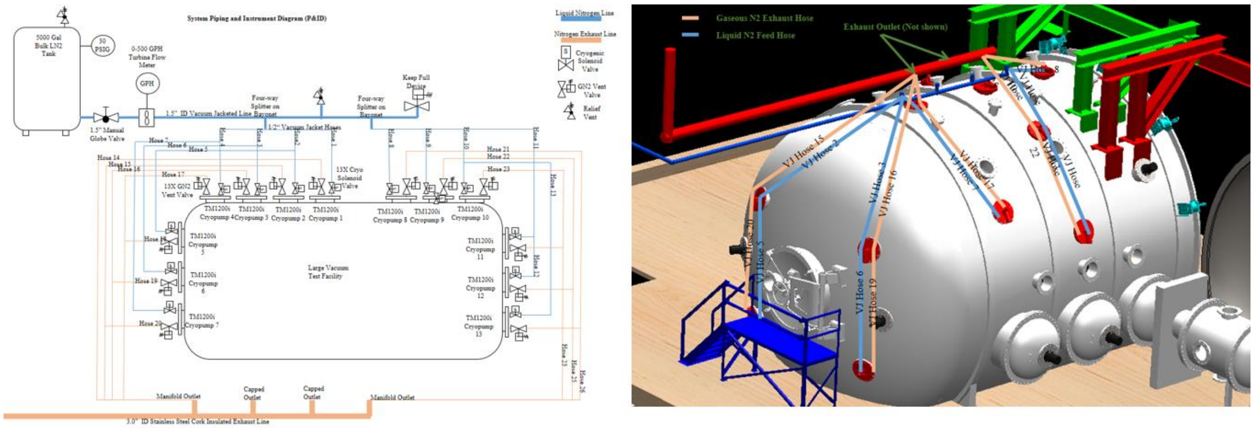

a) b)

Figure 7. Piping and instrument diagram of upgraded plumbing (a) diagram of vacuum jacketed hoses that connect pumps.

To supply the additional TM1200i cryopumps with LN_2, we installed a new vacuum jacketed 3.8 cm ID line to replace the existing 1.3 cm ID insulated copper feed line. The new LN_2 distribution diagram is detailed in Fig. 7. From the main feed line, cryogenic solenoid valves connect to individual TM1200i cryopumps with 1.3 cm vacuum jacket hoses. Significant extra capacity is available to be sourced from the main LN_2 trunk for future projects. The main feed line as installed is shown in Fig 8.

Figure 8. Vacuum jacket line installed over the chamber.

A new centralized 150 kW chiller supplies chilled water to cryopump compressors located in the facility basement. A new insulated stainless steel line exhausts nitrogen vapor from cryopump shrouds. Three 100A 3Ph/480VAC circuits power the chiller and the additional twelve cryopumps.

a) b)

Figure 9. Fourteen new 12 ASA ports cut (a) and installed (b) into vacuum vessel.

To support installation of the additional cryogenic vacuum pumps, twelve 12ASA stainless steel ports were TIG welded through the 2.5 cm thick chamber wall as shown in Fig. 9. The cryopump helium compressors were centralized on rolling carts beneath the vacuum chamber as shown in Fig 10. Each cryopump has two independent cryogenic diodes. On the PEPL cryopump, one diode is placed on the cryocooler heat exchanger and the other is on the plate edge. For the TM1200i, the temperature diodes redundantly measure the cold plate. A new temperature monitoring system consisting of two Lakeshore 224 units was installed in a rack in the basement along with the control switches for the LN_2 solenoid valves. Both the vacuum chamber and the 5000 gallon LN_2 supply tank were given fresh coats of marine grade epoxy paint.

Figure 10. Cryopump helium compressors centralized to the PEPL basement.

C. Development of the PEPL cryopump

A PEPL cryopump was prototyped and tested early in the project. The prototype pumping plate was fabricated from 0.63 cm thick, 1.02 m diameter plate made from aluminum alloy 1100. Alloy 1100 is very close to pure aluminum and therefore has a high thermal conductivity compared with other aluminum alloys at cryogenic temperatures. A copper spreader plate shown in Fig. 11a was added to increase thermal conductivity in the center of the plate. A multilayer insulation (MLI) blanket shown in Fig. 11a was fabricated for the backside of the plate. This MLI blanket was added to eliminate thermal radiation from the backside of the pumping plate to the wall. This surface would not add significant pumping speed due to conductance losses and if left uncovered would essentially be wasted. It was therefore covered with MLI. This approach to radiatively insulate the rear of the plate, allows for surface area to be expanded on the front of the plate. The prototype cryopump (Fig. 11b) was installed into the LVTF side chamber (Fig. 11c). The prototype's pumping speed was measured in excess of 50 kl/s, but the plate would quickly show a large thermal gradient as propellant accumulated. During one test campaign, for example, the entire cold plate started at approximately 30 K without any propellant. After adding 100 L of CO_2 ice to the plate, the plate edge increased to 60 K while the center of the plate was still at 32 K. While this prototype provided useful experience and proof of concept, the thermal conductivity of the pumping plate was deemed insufficient for the final design.

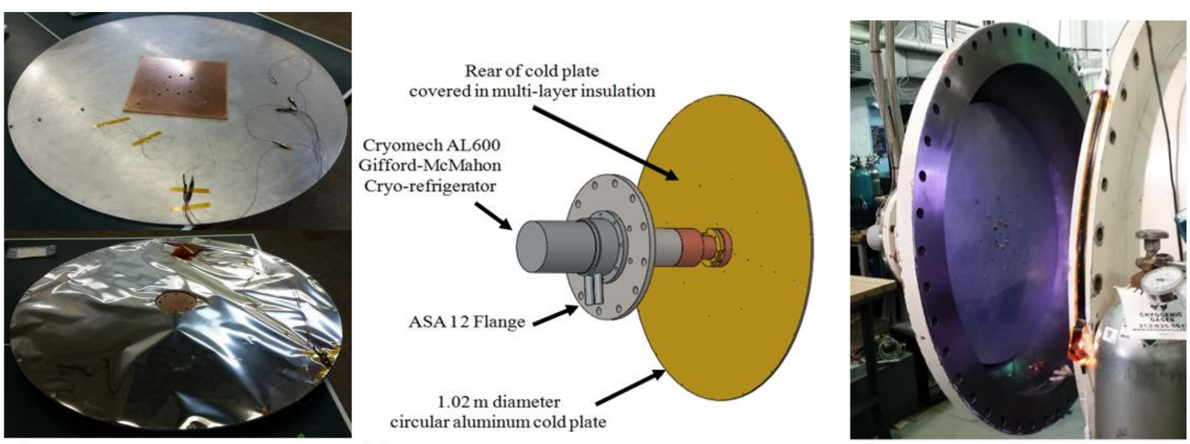

a) b) c)

Figure 11. Prototype PEPL cryopump pumping plate with and without the multilayer insulation (a), overall diagram of the prototype cryopump (b), and final installation of the prototype in the Junior vacuum chamber.

Following the testing of the prototype PEPL cryopump, a thermal modeling effort was carried out to optimize the thermal conductivity of the pumping plate. Solidworks software was used to model the temperature drop across the plate for the prototype. A series of assumptions were made for the model as is follows. Emissivity of the front of the plate was set to 1. This is the worst case condition for radiative heat transfer. In this case, room temperature would produce a total radiative load of approximately 370 W distributed evenly over the front surface of the prototype

pumping plate. Thermal radiative load to the rear of the plate was assumed to be zero due to the MLI blanket covering the back side of the plate. The aluminum pumping panel was given a thermal conductivity of 218 W/mK and the copper heat spreader was given a thermal conductivity of 400 W/mK. The simulated temperature across the plate is shown in Fig. 12. For the model, the cryocooler's copper heat exchanger was set to a constant of 32 K, as was the observed result from the prototype test campaign. As can be seen in the figure, using the assumptions as stated, the temperature drop was modeled to be 42 degrees across the plate. This result affirmed the experimental results on the prototype. Following confirmation that the plate thermal conductivity was not sufficient and that we had a validated method to model temperature drop of any given plate, we parametrically investigated a series of thirty different designs exploring the effect of different plate geometries, diameters, thicknesses, and materials. Within this trade-space, we targeted a design that would minimize temperature drop across the pumping plate at the full radiative load, while also maximizing surface area. Practical considerations including simplicity of the design, availability and cost of plate stock material, and geometry for fitting into the LVTF 48ASA caps were all factors. Three materials were considered: aluminum 1100, copper 101, and copper 110. With the assumed emissivity of 1 and using the room temperature thermal conductivities for aluminum and copper as outlined above, the goal was to keep the edge of the pumping plate around 50 K. Both of these assumptions are conservative. The actual emissivity will not be a perfect 1, and the thermal conductivity of pure copper and pure aluminum increase dramatically at these cryogenic temperatures. This can significantly decrease the temperature drop across the plate and improve functionality in the real plate. For the modeling effort, the temperature of the cryocooler heat exchanger was assumed to increase to 40 K. The load on the cryocooler would increase as the thermal conductivity of the plate was increased. As more load is placed on the cryocooler, the temperature of the heat exchanger increases as is outlined in AL600 capacity curve shown in Fig. 4.
The additional thermal conductivity to the plate would transfer more load to the cryocooler and therefore, a higher temperature (40 K) for the cryocooler heat exchanger was selected based on the capacity curve.

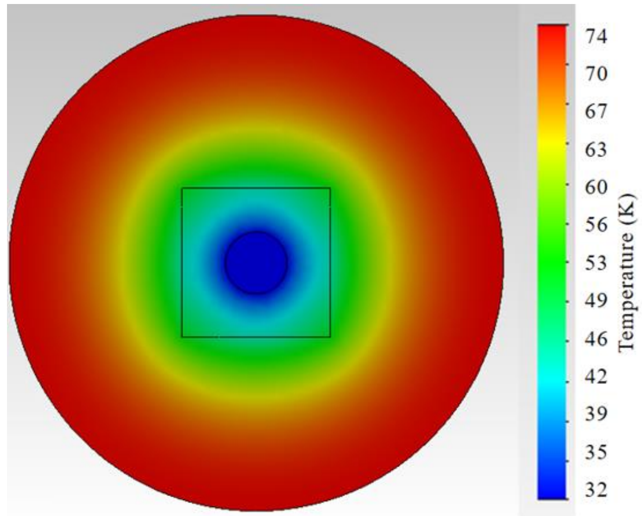

Figure 12. Solidworks thermal model of the prototype pumping panel.

D. Final design for the PEPL cryopump

Based upon the thermal modeling effort outlined in the previous section, a final design for the six PEPL cryopumps was selected. The thermal model for this design is shown in Figure 13.

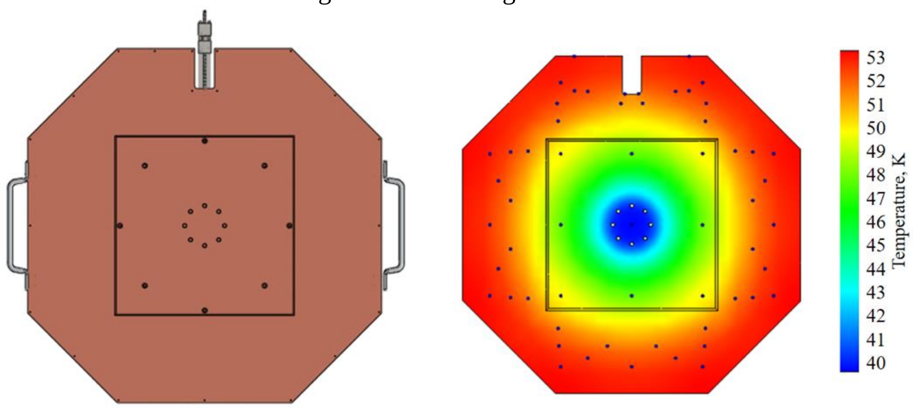

Figure 13. Final design and thermal model of the PEPL cryopump.

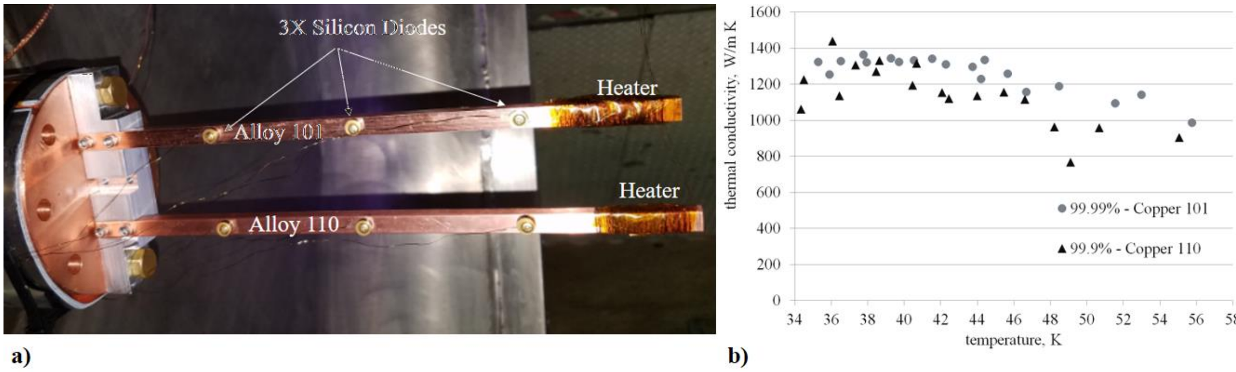

Figure 14. Measuring thermal conductivity of copper alloy 101 and copper alloy 110.

For purposes of the choosing final material spec for the copper, an experiment was carried out to measure the actual cryogenic thermal conductivities of copper alloy 101 (99.99% Cu) vs. copper alloy 110 (99.9% Cu). Figure 14a shows the setup where a square rod of each alloy was attached to the cryocooler on one side and a heating element was wrapped on the other end. Each rod has three silicon diodes spaced 7.6 cm apart.

Applying Fourier's Law $Q = kA\left(\frac{dT}{dx}\right)$, a known input power (Q) could be applied to the heating element in order to drive a thermal gradient (dT/dx) in the rod. Given the known cross sectional area of the rod (A), thermal conductivity (k) can be measured over a range of cryogenic temperatures by altering heater input power. Figure 14b shows thermal conductivities computed for the two alloys over the range of temperatures from 34 to 58 K. Both alloys showed thermal conductivities in excess of 1000 W/mK in the relevant temperature range. Since both alloys showed excellent thermal conductivities, alloy 110 was selected for the plate materials as it is significantly cheaper than alloy 101.

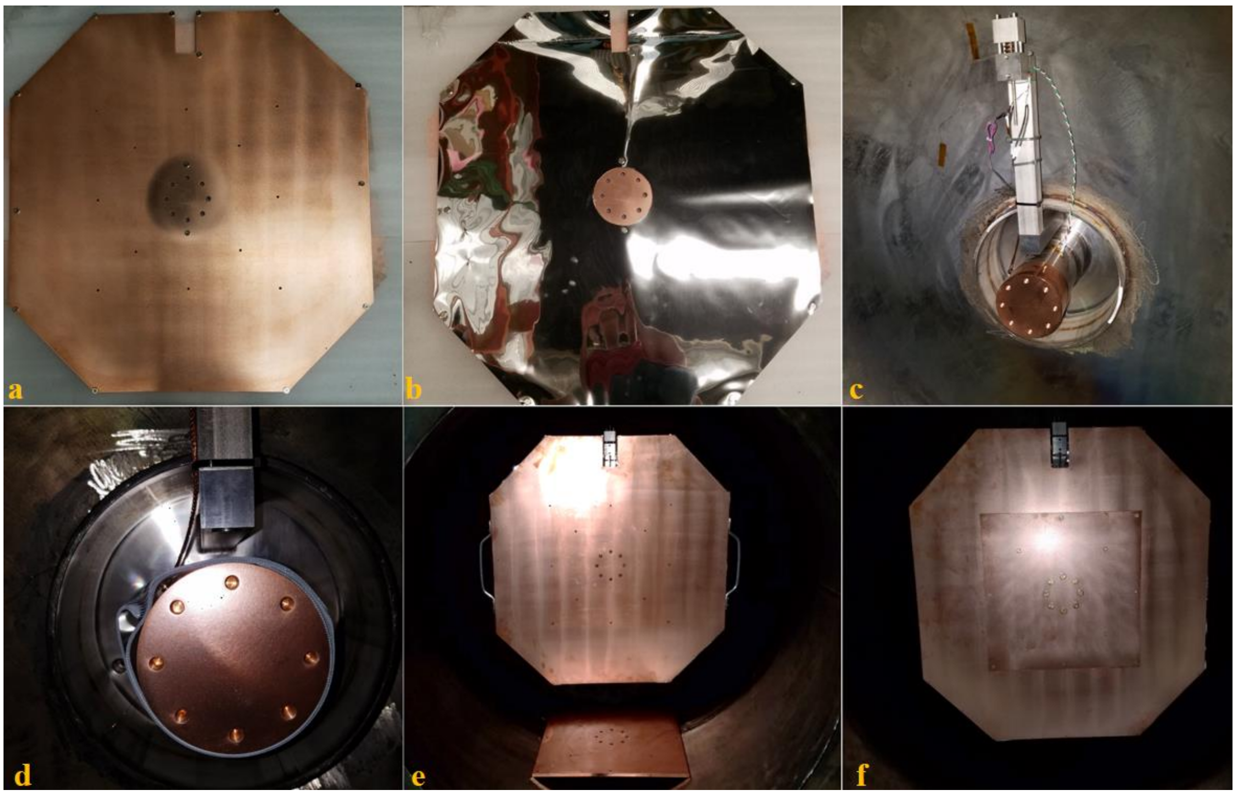

Figure 15. Installation of a PEPL cryopump is shown here. The main pumping plate (a), the attachment of MLI blanket (b), installation of the flange with mechanical support and cryocooler (c), MLI blanket installed on heat exchanger and welded plate support can be seen (d), hanging of the large pumping plate (e), installation of heat spreader and bolting (f).

The assembly of the PEPL cryopump shown in Fig. 15 features a two plate design in order to increase plate thickness in the middle near the cryocooler. The larger plate is roughly octagonal in shape with main dimensions 90 cm tall by 85 cm wide, a thickness of 0.95 cm with a mass of 57 kg. The side of the plate directly facing the chamber wall is covered in a 16 layer MLI blanket. The blanket attaches to the plate with magnets, this eliminates radiation to the rear of plate. The AL600 cryocooler is only rated to carry a load of 18 kg in this configuration, therefore a low thermal conductivity mechanical support system was designed and welded into the feedthrough flange in order to transfer the load of the pumping plate from the cryocooler to the feedthrough plate. The entire plate is suspended by a ¼-20 stainless steel rod that threads into the top of the copper plate. Very little power is lost to conduction through this mechanical support. A separate MLI blanket covers the copper heat exchanger. The second copper plate is 46 cm by 46 cm with a thickness of 0.95 cm has a mass of 18 kg. This smaller plate bolts to the center of the larger plate. Finally two cryogenic diodes are installed onto the cryopump, one to monitor the temperature of the AL600 heat exchanger and one to monitor the temperature at the edge of the pumping plate.

E. The upgraded LVTF side chamber (Junior)

One PEPL cryopump was installed into the Junior facility. This chamber, which is attached to the LVTF through a 60 cm gate valve is valuable for testing small thrusters and cathodes at relevant pressures. The gate valve can be opened during testing, but adds insignificant additional capacity to or from the main chamber, due to conductance limitations of the gate valve. Including its turbopump, Junior now has 41,600 l/s of pumping speed for xenon installed. A brief test campaign characterizing the propellant capacity and thermal conductivity of the PEPL cryopump was carried out in this facility. The setup for the test campaign is shown in Fig. 16, results are outlined in section IV, subsection D.

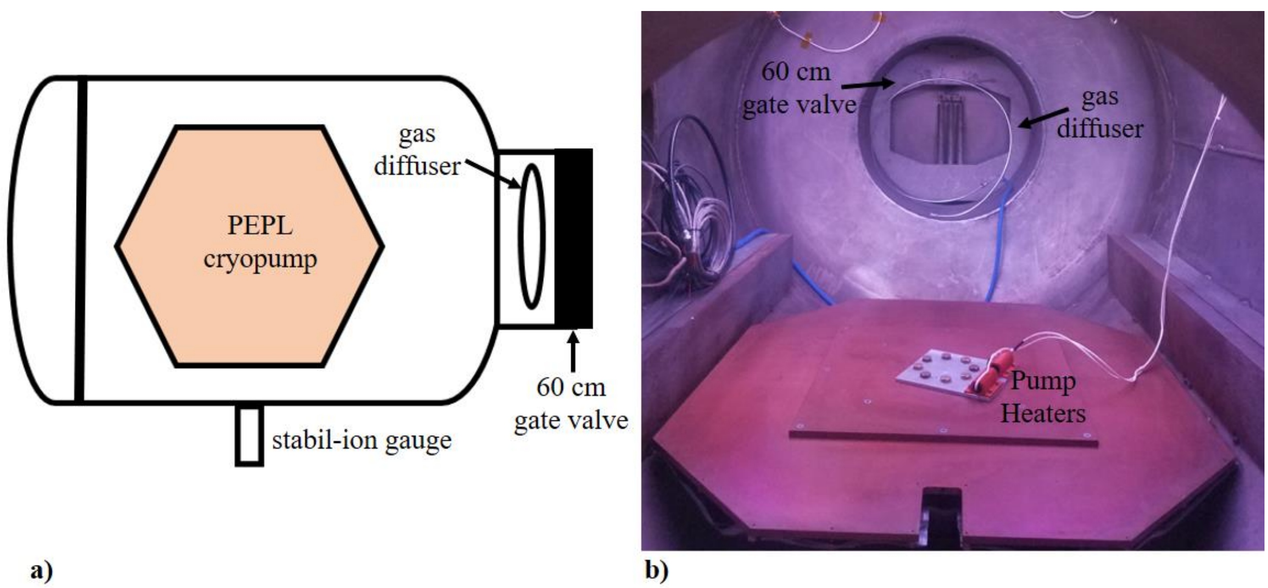

Figure 16. LVTF side chamber (Junior) upgraded configuration.

IV. Results and discussion

A. The LVTF upgraded performance

For xenon

Pumping speed measurements for a variety of different HET hot flow conditions that vary power level, flow rate, and voltage are tabulated in Table 1. All test cases listed in this table represent the full pumping potential for the facility using all eighteen cryopumps. There is some variation in the measured effected pumping speeds for the different test cases, but in general for an operating HET, the effective pumping speed as measured at the thruster is around 500 kl/s for xenon. There are several test cases such 1.3, 1.5 and 1.7 that show a higher effective pumping speed and these cases are associated with operating just the hollow cathode and not the HET. Additionally, the test case where downstream gas injection was used during the firing of a HET (test case 1.6), also shows increased pumping speed. Comparisons between effective pumping speed for differing flow rates and power levels over the course of a one day test campaign (test cases 1.8 – 1.13), show small pumping speed variations between different operating conditions for the HET. All six cases agree on pumping speed within +/- 5 kl/s (+/- 1%).

Table 1. Tabulated effective pumping speed for HET test cases using all eighteen vacuum pumps for xenon.

Test Case	Test Condition	Flow Rate (sccm at 298 K)	Base Pressure (torr-xe)	Pressure at Thruster (torr-xe)	Pumping Speed (l / s)
1.1	hall thruster operation at 7.0 kW, 600 V	163.7	8.20E-08	4.26E-06	496,500
1.2	hall thruster operation at 6.0 kW, 300 V	217.0	8.20E-08	5.83E-06	478,200
1.3	cathode only	21.8	8.20E-08	6.00E-07	533,900
1.4	hall thruster operation at 5.0 kW, 300 V	181.2	7.00E-08	4.88E-06	477,200
1.5	cathode only	16.4	7.00E-08	4.00E-07	628,500
1.6	case 1.4 with downstream injection	389.6	7.00E-08	8.93E-06	557,000
1.7	cathode only	16.4	3.80E-08	4.15E-07	550,200
1.8	hall thruster operation at 3.0 kW, 300 V	134.3	3.80E-08	3.36E-06	512,000
1.9	hall thruster operation at 6.0 kW, 300V	223.1	3.80E-08	5.50E-06	517,400
1.10	hall thruster operation at 6.0 kW, 400V	188.4	3.80E-08	4.70E-06	511,900
1.11	hall thruster operation at 7.5 kW, 500V	190.4	3.80E-08	4.83E-06	503,300
1.12	hall thruster operation at 9.0 kW, 600V	196.2	3.80E-08	4.91E-06	510,000
1.13	hall thruster operation at 9.0 kW, 800 V	162.0	3.80E-08	4.05E-06	511,500

Figure 17 shows the expected pressure curve as measured at the exit plane of an operating HET over a wide range of xenon flow rates for the LVTF. To provide context for 500,000 l/s effective pumping speed, several relevant Hall thruster operating points are provided. For example, a hypothetical 1 kW constellation HET operating at a flow rate of 3 mg/s has a measured pressure around 1 µTorr Xe. NASA's AEPS operating at its highest power operating point of 12.5 kW and 23 mg/s would see 6.5 µTorr.[17] Finally, the highest thrust point demonstrated for the X3 HET at NASA VF-5 of 99 kW and 236 mg/s would see around 65 µTorr[4]. This is in comparison to a measured pressure of 42 µTorr that was recorded during the test in VF-5. Recommended pressure requirements for HET performance (< 30 µTorr) and for near-field plume studies (< 13 µTorr) are shown as well[18].

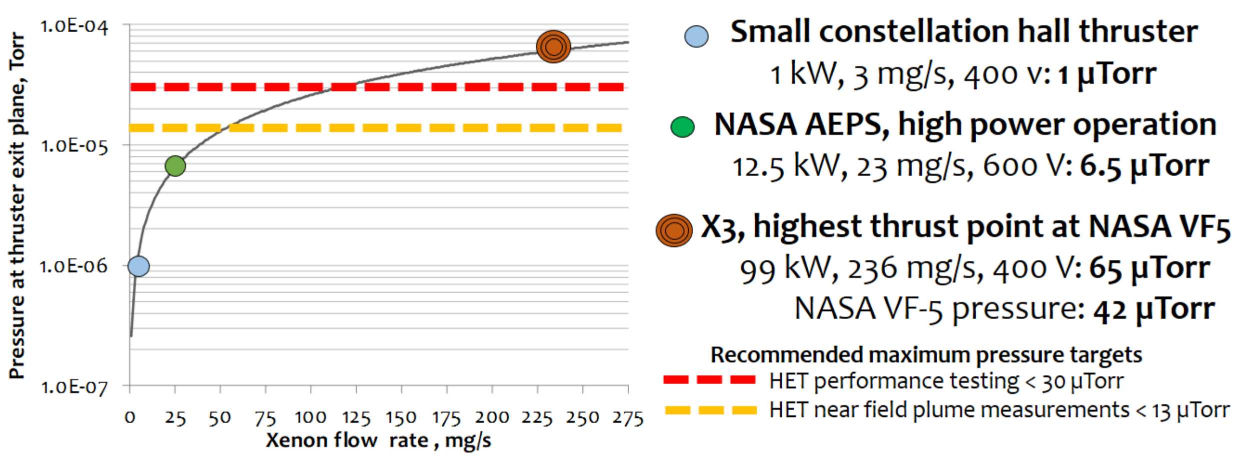

Figure 17. Pressure at the thruster versus mass flow in mg/s xenon for 500 kl/s effective pumping speed. Shows pressure associated with several different operating points for various sizes of hall thruster.

There is significant difference in the measured effective pumping speed for cold flow as compared to hot flow from an operating HET. The pressure with identical mass flows was measured by our gauge to be higher during HET operation than during cold flow. This discrepancy is present both at the Stabil-ion gauge near the exit plane of the thruster as well as a separate Stabil-ion gauge mounted to the chamber wall. One possible source of this discrepancy could be the difference in temperature of the background neutral gas in the chamber. During cold flow, all neutral gas in the chamber should be around the same temperature as the walls of the chamber. This condition is identical to the thermal environment during gauge calibration. During HET operation, after ions are reflected off the beam dump, neutrals may still have significantly more energy than room temperature gas. Therefore on average, background gas in the chamber might be higher during HET operation than during cold flow. If average gas temperature in the vacuum chamber (T_{ch}) is significantly higher than the gas temperature inside the vacuum gauge (T_{ig}), the thermal transpiration effect would cause the gauge to report a spuriously high value.

To correct this effect, the number density inside the gauge (n_{ig}) relates to the number density in the chamber (n_{ch}) as equation 2[19]. While T_{ig}, is generally assumed to be the temperature of the ion gauge walls, T_{ch} may be different from the temperature of the chamber walls since much of the neutral gas is directly rebounding off the beam dump and potentially on average not yet thermalized to the chamber wall temperature. T_{ch} is not directly measured in this work. Future work will seek to measure T_{ch} in order to determine if thermal transpiration is responsible for the pressure disagreement between hot and cold flow.

$$n_{ig} = n_{ch}\sqrt{\frac{T_{ch}}{T_{ig}}} \quad (2)$$

Alternatively, another possible source of the discrepancy could be shifting or directional neutral gas flows that change after the HET is switched on. Regardless of the mechanism of action, a separate set of pumping speed measurements is carried out for various cold flow test cases. Pumping speed measurements for three different facility configurations are tabulated in Table 2. The first cryopumping configuration (case 2.1 through 2.8) uses all eighteen cryopumps. The second cryopumping condition in the table (2.9 through 2.16) uses only the thirteen TM1200i cryopumps. The final cryopumping configuration (2.17 through 2.24) uses one TM1200i and five PEPL cryopumps. In the final configuration, one of the TM1200i cryopumps was run in order to remove nitrogen, oxygen, hydrogen from the chamber as the PEPL cryopumps do not pump these gases. The reason for choosing these cold flow configurations was such that the effective pumping speed performance of the PEPL cryopump could be directly compared with the TM1200i. In the final column in the table, an average effective speed per pump is calculated. This metric can be used to directly infer the effective pumping speed performance of the TM1200i as compared with the PEPL cryopump. This average metric can also determine if the PEPL cryopumps design goal to outperform a TM1200i was reached.

For the cold flow test cases outlined in the table, the total facility pumping speed for all eighteen cryopumps peaked at ~600 kl/s (test cases 2.5 through 2.8). The average effective pumping speed per cryopump was approximately 33 kl/s for the eighteen cryopump configuration; 30 kl/s for the thirteen TM1200i pumping configuration, and 37 kl/s for the final configuration with five PEPL cryopumps and a single TM1200i. From this result we can conclude that in our facility, the TM1200i has an average effective pumping speed of 30 kl/s, and PEPL cryopump has an average effective pumping speed of approximately 38.5 kl/s.

Table 2. Tabulated cold flow pumping speeds for three different pumping configurations for xenon.

Test Case	Cryopumping Configuration	Flow Rate (sccm at 298 K)	Base Pressure (torr-xe)	Pressure at Thruster (torr-xe)	Total Pumping Speed (l / s)	Average Pump Speed (l / s)
2.1	13 TM1200i and 5 PEPL cryopumps	10.9	3.80E-07	6.30E-07	553,100	30,800
2.2	13 TM1200i and 5 PEPL cryopumps	21.8	3.80E-07	8.66E-07	569,000	31,700
2.3	13 TM1200i and 5 PEPL cryopumps	32.7	3.80E-07	1.11E-06	568,300	31,600
2.4	13 TM1200i and 5 PEPL cryopumps	43.7	3.80E-07	1.37E-06	558,700	31,100
2.5	13 TM1200i and 5 PEPL cryopumps	54.6	3.80E-07	1.54E-06	596,000	33,200
2.6	13 TM1200i and 5 PEPL cryopumps	81.9	3.80E-07	2.11E-06	599,500	33,400
2.7	13 TM1200i and 5 PEPL cryopumps	109.2	3.80E-07	2.66E-06	606,500	33,700
2.8	13 TM1200i and 5 PEPL cryopumps	163.7	3.80E-07	3.79E-06	608,300	33,800
2.9	13 TM1200i	10.9	7.00E-08	4.14E-07	402,000	31,000
2.10	13 TM1200i	21.8	7.00E-08	7.93E-07	382,500	29,500
2.11	13 TM1200i	32.7	7.00E-08	1.17E-06	377,100	29,100
2.12	13 TM1200i	43.7	7.00E-08	1.58E-06	366,300	28,200
2.13	13 TM1200i	54.6	7.00E-08	1.94E-06	369,700	28,500
2.14	13 TM1200i	81.9	7.00E-08	2.70E-06	394,300	30,400
2.15	13 TM1200i	109.2	7.00E-08	3.60E-06	391,700	30,200
2.16	13 TM1200i	163.7	7.00E-08	5.38E-06	390,600	30,100
2.17	1 TM1200i and 5 PEPL cryopumps	10.9	3.75E-07	1.02E-06	214,400	35,800
2.18	1 TM1200i and 5 PEPL cryopumps	21.8	3.75E-07	1.67E-06	213,600	35,600
2.19	1 TM1200i and 5 PEPL cryopumps	32.7	3.75E-07	2.32E-06	213,300	35,600
2.20	1 TM1200i and 5 PEPL cryopumps	43.7	3.75E-07	3.00E-06	210,700	35,200
2.21	1 TM1200i and 5 PEPL cryopumps	54.6	3.75E-07	3.65E-06	211,100	35,200
2.22	1 TM1200i and 5 PEPL cryopumps	81.9	3.75E-07	4.98E-06	225,200	37,600
2.23	1 TM1200i and 5 PEPL cryopumps	109.2	3.75E-07	6.55E-06	224,000	37,400
2.24	1 TM1200i and 5 PEPL cryopumps	163.7	3.75E-07	9.66E-06	223,400	37,300

One interesting note regarding all three cryopumping configurations is that there is a discontinuity in the facility performance between the 43.7 sccm and 54.6 sccm or alternatively between the 54.6 and 81.9 flow point. At the higher flow rates, the facility performance is better. For example, test case 2.4 at 43.7 sccm shows an effective pumping speed 559 kl/s for the chamber, while test case 2.5 at 54.6 sccm shows an effective pumping speed of 596 kl/s. This is a pumping speed difference of approximately 40 kl/s, and this discontinuity is present for all three cryopumping configurations. It is important to note that two different flow controllers were used for each test series, a flow controller is attached to the cathode of the thruster and a separate flow controller is attached to the anode. The cold flow conditions first started using the cathode up to 43.7 or 54.6 sccm point and then added in flow to the anode for the higher flow conditions. However, since both flow controllers were recently calibrated against the same dry calibration system, bad calibrations for the flow controllers can be ruled out as the source of difference. The most logical source of the difference is that cold flow through the cathode produced different effective pumping speed results as compared with the same flow through the anode due to different flow expansion patterns in the chamber relative to the gauge. This is opposite from the hot flow conditions in which pumping speed tended to be higher for cathode only operation as compared with conditions that has an operating hall thruster.

For krypton

Performance of the upgraded facility was also characterized with krypton propellant during a HET test campaign. The pumping configuration for this test configuration used seventeen cryopumps as one of the PEPL cryopumps was down for servicing. For these results all of the flow controllers were recalibrated for krypton and the ion gauge readings were corrected for krypton. Cold flow effective pumping speed at the thruster was measured to be approximately 660 kl/s at 150 sccm. The pumping speed for an HET with krypton was measured to be 601 kl/s at a flow rate of 276.7 sccm and 6 kW power input. After factoring in the additional PEPL cryopump that was not running for these results, these pumping speed numbers are close to the 25% higher pumping speed on krypton that is expected due to the higher molecular thermal speed of the krypton as compared with xenon. Additionally, this test verifies that the PEPL cryopump works with krypton propellant.

B. LVTF performance during a 100-hour, 1000-liter test campaign of a high-power HET

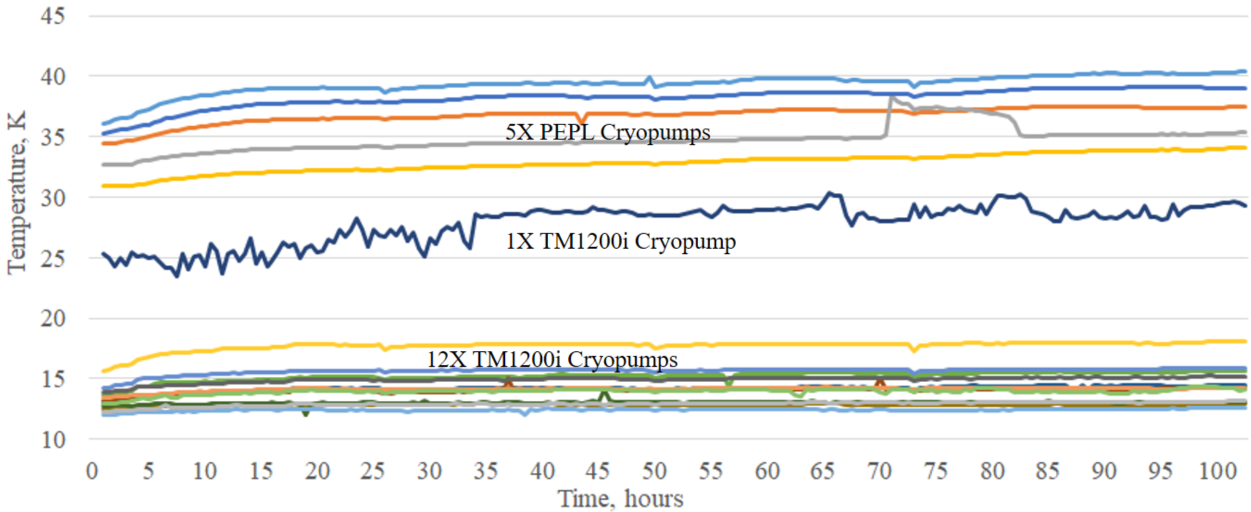

Figure 18. Silicon diode temperatures for all eighteen cryopumps over the 100 hour, 1000 liter test campaign. PEPL cryopumps are reporting the temperature of the plate edge, not the heat exchanger.

A 100 hour continuous test of a Hall thruster operating at 7 kW and flow rate of 163.7 sccm provided an opportunity to characterize the upgraded facility for longer duration testing. The average pumping speed over the duration of the test was found to be 484 kl/s for xenon. There were no observed pressure spikes due to xenon shedding during the campaign. Figure 18 shows the cryopump temperatures as they varied over the 100 hour test. There are generally three groupings of temperature range for the cryopumps as can be seen in the figure. The first group is the 12 TM1200i cryopumps that range from 12 K to 18 K. Secondly there is one TM1200i that tends to operate more erratically between 25 and 30 K, but nonetheless stays cold enough to pump xenon or krypton. Finally there is the PEPL cryopumps which operate from 30 K to 40 K. As can be seen in the data, the PEPL cryopumps have substantial variation in starting temperature due to variations in the specific AL600 cryocooler's cooling capacity. The AL600 cryocoolers have a guaranteed minimum cooling capacity spec, but there seems to be a noticeable amount of variation above the minimum spec. Over the course of the campaign, the edge diode of the PEPL cryopumps increases 3 K to 4 K, however much of this increase in temperature is rapid early in the campaign and stabilizes to a more gradual increase through the end. One of the PEPL cryopumps (gray) had rapid temperature drift that later drifted back down. This episode was not associated with any shedding or other noticeable effect. Table 3 shows the starting and final temperatures of the cryopumps. Cryopump #2 through #6 are the PEPL cryopumps with temperatures measured at the plate edge and #7 though #19 are the TM1200i.

Table 3. Temperature of the LVTF cryopumps at the beginning and end of the 100 hour campaign. Cryopump #2 through #6 are the PEPL cryopumps with temperatures measured at the plate edge and #7 though #19 are the TM1200i.

Cryopump #	2	3	4	5	6	7	8	9	10	11	12	13	14	15	16	17	18	19
Temperature at beginning, K	36.1	34.4	32.7	30.9	35.3	13.6	13.0	13.2	13.9	12.5	25.3	12.7	12.0	13.4	12.3	15.6	14.2	13.0
Temperature at end, K	40.4	37.5	35.3	34.1	39.0	15.7	14.5	14.2	15.2	12.9	29.3	13.1	12.6	14.2	13.1	18.1	15.8	14.2

C. Relative contribution of individual cryopumps to the LVTF's cumulative pumping speed

Over a series of eighteen different HET test days, cold flow and hot flow effective pumping speed measurements were made in order to evaluate relative conductance to each of the cryopumps. Each individual test operated seventeen of the eighteen LVTF cryopumps. The cryopump that was shut down was alternated between tests such that its effective contribution to pumping speed could be characterized. All of the HET flow rate except test case (4.2) are with a thruster operating at an identical operating point and all of the cold flow rates are the same.

Table 4. Facility effective pumping speed comparisons for hot and cold flow. Each test case alternates which cryopump is not operational. Cases that highlighted in green are the most effective cryopumps and red are least effective.

Test Case	Cryopump # Not Running	Base Pressure (torr-xe)	Cold Flow (sccm at 298 K)	Cold Flow (torr-xe)	Thruster (sccm at 298 K)	Thruster (torr-xe)	Cold Flow Pumping Speed (l/s)	Thruster Pumping Speed (l/s)
4.1	2	3.00E-08	183.4	4.49E-06	183.4	5.22E-06	520,823	447,567
4.2	3	3.00E-08	183.4	4.38E-06	171.4	4.71E-06	533,994	463,842
4.3	4	6.40E-08	183.4	4.13E-06	183.4	4.95E-06	571,292	475,414
4.4	5	3.00E-08	183.4	4.40E-06	183.4	4.84E-06	531,550	482,926
4.4	6	3.90E-08	183.4	4.20E-06	183.4	4.78E-06	558,248	489,954
4.6	7	9.60E-08	183.4	4.27E-06	183.4	5.01E-06	556,510	472,705
4.7	8	1.30E-07	183.4	4.31E-06	183.4	4.66E-06	555,711	512,775
4.8	9	1.29E-07	183.4	4.04E-06	183.4	4.84E-06	593,933	493,074
4.9	10	4.40E-08	183.4	3.96E-06	183.4	4.79E-06	593,175	489,438
4.10	11	3.50E-08	183.4	4.40E-06	183.4	5.00E-06	532,158	467,849
4.11	12	6.10E-08	183.4	3.82E-06	183.4	4.88E-06	617,949	482,024
4.12	13	9.00E-08	183.4	3.89E-06	183.4	4.70E-06	611,282	503,877
4.13	14	5.00E-08	183.4	3.87E-06	183.4	4.66E-06	608,082	503,877
4.14	15	7.00E-08	183.4	4.41E-06	183.4	4.77E-06	535,224	494,228
4.15	16	5.00E-08	183.4	4.47E-06	183.4	4.85E-06	525,537	483,932
4.16	17	5.87E-08	183.4	4.49E-06	183.4	4.81E-06	524,196	488,892
4.17	18	8.40E-08	183.4	4.35E-06	183.4	4.85E-06	544,508	487,384
4.18	19	1.20E-07	183.4	4.01E-06	183.4	4.87E-06	597,139	489,026

The data is shown in Table 4. The relative configuration of the cryopumps, hall thruster, and beam dump for the test facility is shown Figure 19 and Figure 5. This test characterized the relative contribution of each individual cryopump to the total effective pumping speed by noting the decrease in effective pumping speed in absence of its operation. For example in test case 4.1 in the table, the overall facility pumping speed as compared with the other facility configurations was slowest for both the cold and hot flow cases. Therefore based on this data, it can be concluded that pump 2 is the highest contributor to the effective pumping speed as compared with any of the eighteen cryopumps. On the other hand, cryopump 13 and 14 appear to be the least contributing because when they are shut down, the overall pumping at the thruster speed remains highest. This method was the least invasive for comparing the effectiveness of individual cryopumps within the context of a fully operational facility and allowed for comparisons during hall thruster firing. The table is color coded for easy viewing with the six most effective cryopumps for both cold and hot flow shown in green and the six least effective shown in red. It interesting to note that the six most effective for cold flow are not the same as the six most effective during firing of a HET. However, there are some pumps which appear in the top six for both hot and cold flow conditions. Pumps 2, 3, and 11 fall into the top six for both hot and cold flow while pumps 9, 13, 14, and 19 fall into the bottom six for both hot and cold flow. Broadly speaking, the data is difficult to interpret. It's clear that the PEPL cryopumps are faster than the Tm1200i. Additionally, it's possible that directional flows within the chamber may play a role.

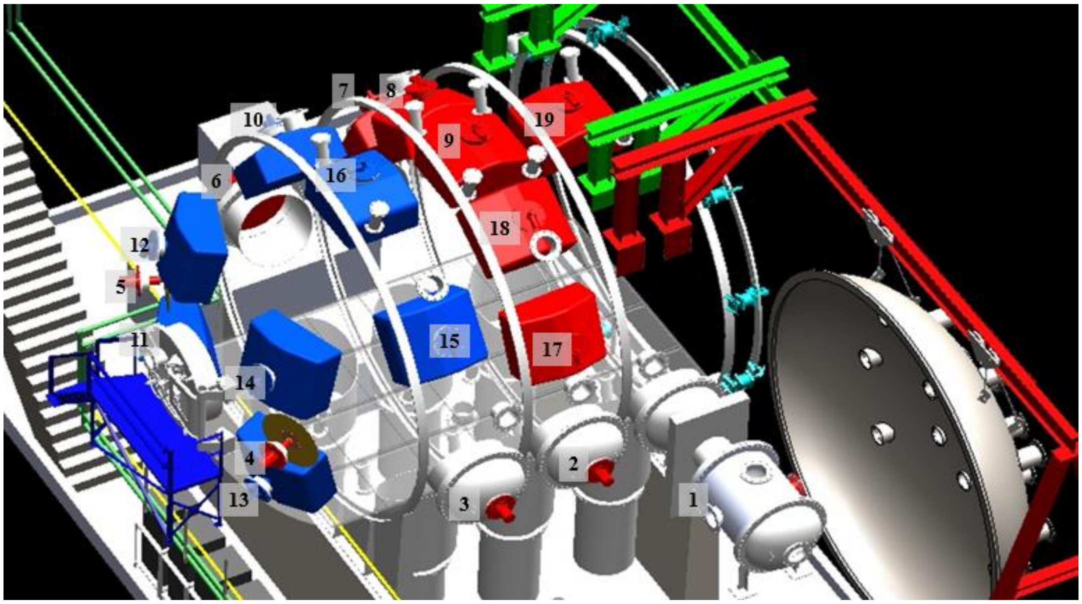

Figure 19. Cryopump number scheme for reference to Table 4.

D. PEPL cryopump performance in the LVTF side chamber

To evaluate the thermal design of the PEPL cryopump as well as to characterize the xenon capacity of the pump, a set of cold flow experiments were conducted in the LVTF's side chamber. Figure 16 shows the general test setup that was used to examine performance of the PEPL cryopump in isolation. All of the data was collected for cold flow testing using an ion thruster gas diffuser located at one end of the vacuum chamber as shown in the figure schematic. The cryopump was installed in a center flange on the bottom the chamber with a diode on the heat exchanger and a diode on the edge of the pumping plate.

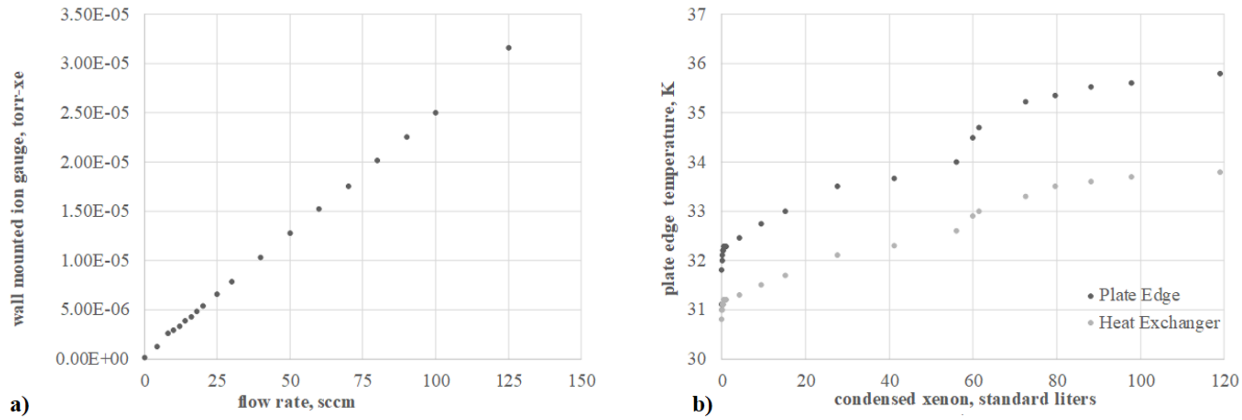

Figure 20. Xenon flow rate (sccm) vs side chamber pressure (a) and condensed xenon on plate vs plate temperature.

Figure 20a shows chamber pressure as a function of propellant flow rate as measured by a Stabil-ion gauge located on the wall of the chamber. The pumping speed computed from the pressure gauge for the chamber is around 50 kl/s for xenon which includes the pumping speed associated with a 2 kl/s turbopump on the top of the chamber. This measured pumping speed which is higher than the theoretical pumping speed is likely due some gas directly impinging on the pump from the gas diffuser and would be less in other chamber configurations. Figure 20b shows the effect on the plate temperature as additional xenon is condensed onto the pumping plate. Throughout the test 120 L of xenon is condensed onto the plate, raising the plate edge from 31.1 K to 35.9 K and the heat exchanger increased from 30.8 K to 33.9 K. This test is significant as it indicates how the PEPL cryopumps would perform in a facility wear tear test campaign. In this case, if 120 L of xenon were deposited on each of the eighteen cryopumps in the LVTF, the main chamber should at least be able to handle 2100 liters prior to regen and likely even more. Figure 21 is before (a) and after (b) the test, as viewed through the chamber view port. Condensed xenon can viewed directly.

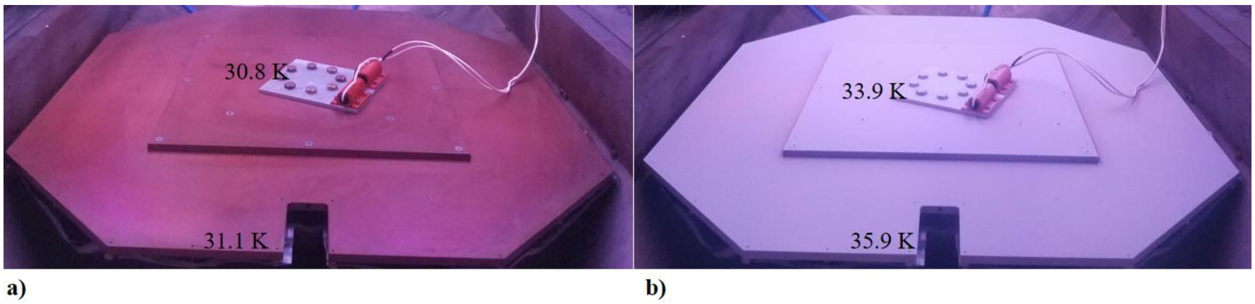

Figure 21. Thermal gradient of the PEPL cryopump before (a) and after (b) condensing 120 l of xenon.

The temperature gradient measured in the pumping plate is 2 K after 120 liters of xenon are condensed. This is significantly less than the 13 K temperature gradient that was predicted in the modeling. This is a very positive result, which we attribute to the increased thermal conductivity of copper at cryogenic temperatures (1000 W/mK vs 400 W/mK) as we had measured in Fig. 14. We likely gained benefit from our assumption of 1 that we choose for the emissivity as well. In either case, the thermal modeling was a tool to get to a robust enough cryopump design to justify the construction of six units prior to the actual testing of the design. Peak pumping performance could likely be increased in a future design. Additionally, there is some variation in the actual performance of each individual AL600 as is shipped from Cryomech and it's important to note that the specific AL600 that is installed into the side chamber produced the most cooling power as compared with the other five units that had been procured. Cyromech guarantees a minimum spec, but many of the cryocoolers in fact produce excess cooling over the minimum spec.

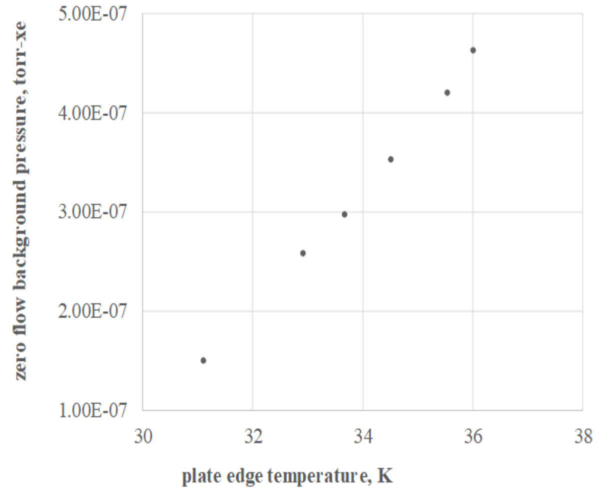

Figure 22. Plate edge temperature vs. zero flow background pressure

At several points during the test, the gas flow and turbopump were sealed off in order to measure the zero flow background pressure in the chamber. Alternatively this can be thought of as being related to the vapor pressure of the xenon in the chamber above the cryopump. Figure 22 shows the measured zero flow background pressure as a function of the plate edge temperature. The general trend shown in the plot is expected in that as more xenon is added to the cryopump, the plate temperature rises and the vapor pressure above the pumping plate also increases.

Similar testing was carried out with krypton propellant in the side chamber where 100 liters of krypton was successfully condensed on to the cryopump at useful background pressure proving this design cryopump also can pump large amounts of krypton with a high pumping speed. Pumping plate thermal gradients reflected similar results as compared with the xenon testing. Additionally, pumping speed was somewhat higher due to the higher thermal speed of krypton.

V. Conclusion

The Large Vacuum Test Facility, a six meter diameter by nine meter vacuum chamber at the University of Michigan has been upgraded to support the testing of next generation electric propulsion systems. The upgraded effective pumping speed for xenon is half a million l/s for xenon for a high-powered HET and upwards of 600, kl/s for cold flow xenon. The upgraded facility also works for krypton with effective pumping speed at the thruster measured at 600 kl/s for an operating HET and 660 kl/s for cold flow. A new LN_2-free cryopump design has been developed at PEPL based upon the AL600 cryocooler from Cryomech. It has a theoretical pumping speed of 39,600 l/s for xenon and six of these cryopumps have been installed into the LVTF and its side chamber. Additionally, six additional TM1200i cryopumps have been installed, bringing the number of large vacuum pumps installed into the LVTF and its side chamber to be nineteen. The supporting infrastructure include LN_2, electrical, process cooling water, and many other facility subsystems have been scaled to support new cryopumps. The performance of chamber has been documented for a 100 hour continuous firing of a high power Hall thruster, where over 1000 liters of xenon were captured by cryopumps without regen or any noteworthy complications.

Acknowledgments

The authors would like to thank the fantastic welder Steve Wise from Erie Technologies for his support in chamber modifications the LVTF and for whom was entrusted with plasma cutting large holes through an irreplaceable high vacuum test facility. Additional thanks to all the current and many former PEPL personnel that assisted on the upgrade project by directly supported this effort through physical labor and discussions. Much of the data presented for this paper was gathered during test campaigns run by Ethan Dale, Sarah Cusson, Matt Byrne, Zach Brown, Marcel Georgin, Josh Woods, and Leanne Su. Thanks to Chuck Garner for feedback on cryopump design and sharing his experience with the installation of the original seven TM1200i cryopumps into the LVTF. Thanks to Costas Tzemos from PHPK and Chao Wang from Cyromech for much support with the cryogenic systems. Thanks to Dean Massey for the very early planning and vision for much of this project. Thanks to Bill Cleveland from Precision Manufacturing for making many of the mechanical components needed for the upgrade. Thanks to Michael Rayle who originally created the invaluable and dimensionally accurate LVTF Solidworks model from original 1960s facility blueprints. Final thanks for a generous loan of four TM1200i cryopumps from the California Institute of Technology NASA Jet Propulsion Laboratory. This work is supported in part by the Air Force Defense University Research Instrumentation Program award no. FA9550-16-1-0275.

References

[1] Herman, D. A., Gallimore, A. D., "Discharge Chamber Plasma Structure of a 30-cm NSTAR-type Ion Engine," 40th Joint Propulsion Conference, Fort Lauderdale, FL, AIAA-2004-3794, July 11-14, 2004.

[2] King, L. B., Gallimore, A. D., and Marrese, C. M., "Transport Property Measurements in the Plume of an SPT-100 Hall Thruster", Journal of Propulsion and Power, Vol. 14, No. 3, 327- 335, May-June 1998.

[3] Welander, B. et al., "Demonstration of the XR-12 Hall Current Thruster," IEPC-2013-451.

[4] Hall, Scott J., "Characterization of a 100-kW Class Nested-Channel Hall Thruster," University of Michigan, Ph.D. Dissertation, 2017.

[5] Hofer, R.R., Cusson, S.E., Lobbia, R.B., and Gallimore, A.D., "The H9 Magnetically Shielded Hall Thruster," IEPC-2017-232, 2017.

[6]J. Dankanich, M. Walker, M. Swiatek and J. Yim, "Recommended Practice for Pressure Measurement and Calculation of Effective Pumping Speed in Electric Propulsion Testing," Journal of Propulsion and Power, 2017.

[7] R. Hofer et al., "The 12.5 kW Hall Effect Rocket with Magnetic Shielding (HERMeS) for the Asteroid Redirect Robotic Mission," AIAA 2016-4825.

[8] R. Hofer, S. Cusson, R. Lobbia, and A. Gallimore, "The H9 Magnetically Shielded Hall Thruster," IEPC-2017-232.

[9] S. Hall et al., "High Power Performance of a 100-kW Class Nested Hall Thruster," IEPC-2017-228.

[10] D. Byers and J. 5anich, "A Review of Facility Effects on Hall Effect Thrusters," IEPC-2009-076.

[11] H. Kamhawi et al., "Performance, Facility Pressure Effects, and Stability Characterization Tests of NASA's Hall Effect Rocket with Magnetic Shielding Thruster," AIAA-2016-4826.

[12] K. Diamant, R. Spektor, E. Beiting, J. Young and T. Curtiss, "The Effects of Background Pressure on Hall Thruster Operation," AIAA-2012-37235.

[13] R. Hofer and J. Anderson, "Finite Pressure Effects in Magnetically-Shielded Hall Thrusters,"AIAA-2014-3709.

[14] R. Spektor, W. Tighe, and H. Kamhawi, "Laser Induced Fluorescence Measurements in a Hall Thruster as a Function of Background Pressure," AIAA-2016-4624.

[15] C. Garner et al., "Methods for Cryopumping Xenon," AIAA-1996-3206.

[16] Cryomech, "AL200 Cryorefrigerator Capacity Curve."

[17] R. Hofer et al., "Development Status of the 12.5 kW Hall Effect Rocket with Magnetic Shielding (HERMeS)," IEPC-2017-231.

[18] J. Dankanich, M.Walker, M. Swiatek, J. Yim, "Recommended Practice for Pressure Measurements and Calculation of Effective Pumping Speeds during Electric Propulsion Testing," IEPC-2013-358.

[19] K Jousten, "Temperature corrections for the calibration of vacuum gauges," Vacuum, 1998.